PCCP

ROYAL SOCIETY OF CHEMISTRY

PAPER

View Article Online
View Journal

Cite this: DOI: 10.1039/d1cp05537b

Weak nuclear spin singlet relaxation mechanisms revealed by experiment and computation†

Boris Kharkov,[a] Xueyou Duan,[b] Jyrki Rantaharju,[c] Mohamed Sabba,[c] Malcolm H. Levitt,[c] James W. Canary[b] and Alexej Jerschow *[b]

Nuclear spin singlet states are often found to allow long-lived storage of nuclear magnetization, which can form the basis of novel applications in spectroscopy, imaging, and in studies of dynamic processes. Precisely how long such polarization remains intact, and which factors affect its lifetime is often difficult to determine and predict. We present a combined experimental/computational study to demonstrate that molecular dynamics simulations and *ab initio* calculations can be used to fully account for the experimentally observed proton singlet lifetimes in ethyl-d_5-propyl-d_7-maleate in deuterated chloroform as solvent. The correspondence between experiment and simulations is achieved without adjustable parameters. These studies highlight the importance of considering unusual and difficult-to-control mechanisms, such as dipolar couplings to low-gamma solvent nuclei, and to residual paramagnetic species, which often can represent lifetime limiting factors. These results also point to the power of molecular dynamics simulations to provide insights into little-known NMR relaxation mechanisms.

Received 4th December 2021,
Accepted 25th February 2022

DOI: 10.1039/d1cp05537b

rsc.li/pccp

1 Introduction

The ability of nuclear spin singlet order (SO) to exhibit lifetimes much longer than spin lattice relaxation times has motivated the investigation into the use of such states as information or polarization storage vehicles.[1–3] Potential applications include imaging,[4] the study of slow kinetic or dynamic processes,[5,6] or the study of weak relaxation mechanisms.[7,8]

The mechanisms that ultimately lead to the decay of SO are often difficult to identify and quantify. Molecular dynamics (MD) and *ab initio* calculations (including *ab initio* MD) have been used for the calculation, prediction, and analysis of NMR processes,[9–15] but this approach has not been extended to nuclear spin singlet states, with the exception of the work of Håkansson.[16] That work presented a unique approach to use a fitting algorithm to interpolate between different MD snapshots for which *ab initio* quantities were calculated. In that work, the spin rotation, chemical shift anisotropy and intramolecular dipolar mechanisms were calculated, but intermolecular mechanisms were not included. As shown below, intermolecular mechanisms can represent major components of the relaxation rate constants, and can represent lifetime limiting factors.

Here, we report on nuclear spin singlet lifetime measurements in ethyl-d_5-propyl-d_7-maleate in deuterated chloroform as solvent at different temperatures, and calculate the underlying singlet relaxation mechanisms using MD simulations and *ab initio* calculations. MD simulations are used, in particular, to derive quantities for the intermolecular dipolar coupling mechanism due to nuclei in solvent molecules (^{2}H, ^{35}Cl, ^{37}Cl). Another significant effect is given by chemical shift anisotropy (CSA), which is treated using a combination of *ab initio* calculations and MD simulations.

In addition, the paramagnetic mechanism due to dissolved oxygen is modeled as a dipolar coupling mechanism to a spin-1 object with an electronic relaxation time obtained from the literature. Paramagnetic relaxation is potentially a very complex subject, and we highlight below the simplifying assumptions and justifications used in order to make the calculation of this effect from MD trajectories tractable. The paramagnetic effect is further treated in a self-consistent manner, by extracting a scaling factor from its contribution to solvent spin–lattice relaxation.

Overall, the calculation of all these mechanisms accounts for the measured rate constants over the temperature range considered. This work points, in particular, to the fact that dipolar interactions with low-gamma nuclei, such as ^{2}H, ^{35}Cl, and ^{37}Cl of the solvent could ultimately be lifetime limiting factors in the quest for the longest nuclear spin singlet lifetimes in solution.

[a] *Laboratory of Biomolecular NMR, St. Petersburg State University, St. Petersburg 199034, Russia*
[b] *Department of Chemistry, New York University, New York, NY 10003, USA. E-mail: alexej.jerschow@nyu.edu*
[c] *School of Chemistry, University of Southampton, Southampton, UK*

† Electronic supplementary information (ESI) available. See DOI: 10.1039/d1cp05537b

2 Experimental

2.1 Synthesis and sample preparation

All experiments were performed on a degassed 5.4 mM solution of the ethyl-d_5 propyl-d_7 maleate (EPM) molecule in $CDCl_3$. The nuclear spin singlet order (SO) was produced between the vinylene protons of EPM. The side chains (ethyl and propyl) were deuterated. The synthesis and sample preparation were performed in analogy to the previously described procedure,[17,18] but the details are reproduced here for convenience.

All reagents were purchased from commercial sources and used without further purification. Maleic anhydride and anhydrous ethanol-d_6, were purchased from Sigma Aldrich. *n*-Propyl-d_7 alcohol was purchased from C/D/D isotope. Triethylamine was purchased from Fisher Scientific. All NMR solvents were purchased from Cambridge Isotopes. Deuterated asymmetric maleate acid esters were synthesized from maleic anhydride by following the procedure in the literature.[17] All reactions sensitive to moisture were done under inert atmosphere (Ar protection) with the use of anhydrous solvents taken from a standard solvent-drying system. $CDCl_3$ was obtained from Sigma Aldrich at $>99.8\%$ purity. Constricted sealable NMR tubes were purchased from Norell. Samples were dissolved in deuterated chloroform and subjected to 5 cycles of freeze–pump–thaw degassing and the NMR tubes were subsequently flame-sealed.

The height of the solution in the NMR tube was approximately 9 mm and the tube was positioned such that it fit completely within the coil volume to avoid convection artifacts.[18]

2.2 NMR spectroscopy

All NMR measurements were performed on the same degassed sample as described above to ensure the same amount of dissolved oxygen. The chloroform ^{1}H T_1 measurements were performed using the residual $CHCl_3$ signal in the $CDCl_3$ solvent ($<0.2\%$). The maleate T_1 and T_S measurements were performed on the vinylene protons of the deuterated EPM solute.

The experiments were performed on a Bruker AV500 (500 MHz, 11.74 T) spectrometer with a broad-band direct observe probe. Table 1 lists the pulse sequence parameters optimized for the sequence shown in Fig. 1. The pulsed field gradients for the T00 filter were set to 35, 30, and 25% of the maximum setting (≈ 0.5 T m^{-1}) and their durations were set to 2.4, 1.6, and 1 ms, respectively, to avoid accidental refocusing of quenched magnetization components. The $\pi/2$ flip angle durations ranged from 16.1–17.5 μs.

Table 1 Pulse sequence parameters for singlet measurements. n_1, n_2, and Δ are the M2S loop and delay parameters corresponding to Fig. 1. τ_p is the $\pi/2$ pulse duration, n_s the number of scans, and T_r the recycle delay

T/K	n_1	n_2	Δ/ms	τ_p/μs	n_s	T_r/s
233.15	10	5	20.65	17.0	4	25
253.15	23	11	20.65	16.9	4	35
283.15	26	13	20.60	17.4	4	50
298.15	18	9	20.25	16.1	6	45

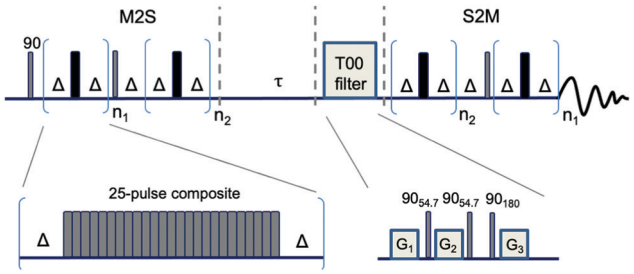

Fig. 1 M2S-S2M sequence with zero-rank (T00) filter[19] and 25-component composite pulses (for convection compensation).[18]

The chemical shift difference between the two vinylene protons was determined from the M2S optimization parameters as listed in Table 1. The shift differences $\Delta\delta$ varied with temperature and the usable range was 0.5–2 Hz. The $\Delta\delta$ values are shown in Fig. S1 (ESI†). Between the temperatures 253 and 283 K, the difference was found to be too small to efficiently generate SO. The M2S parameters were optimized for each temperature and are given in Table 1.

For T_1 measurements, the saturation-recovery sequence was used with a T00 filter for the saturation step.

2.3 Computational

Molecular dynamics (MD) simulations were performed using Amber20.[20] The system was prepared in antechamber using bcc charges, and the general Amber force field (GAFF[21]) was used for parameterization. The EPM molecule was prepared and solvated by $CHCl_3$ in an isotropic box of 50 Å side length using Amber's antechamber and tleap programs. The box also contained one O_2 molecule to model paramagnetic relaxation due to oxygen. Following that, the system energy was minimized using 3000 steps with the steepest descent method and 2000 steps with the conjugate gradient method. The system was subsequently heated to the desired temperature in 20 000 steps. Temperature stabilization was performed using a Langevin thermostat with collision frequency of 5 ps^{-1}. A stabilization run was performed at the target temperature at constant temperature and pressure for 100 000 steps. Pressure regulation was performed using a Berendsen barostat with a pressure relaxation time of 1 ps. Following that, a restart file was saved after every 50 000 steps (to give a total of 100 restart snapshots as samples of an isothermal–isobaric (*NPT*) ensemble). Each of the snapshots was used for a short CPU production run of 20 000 steps using unconstrained microcanonical (*NVE*) ensemble conditions. Following that, a production run of 10 million steps was performed using Amber's GPU code (pmemd.cuda) for each of the samples. A timestep of 0.2 fs and a cutoff of 11 Å for electrostatic interactions were used throughout. Periodic boundary conditions were used for heating, stabilization, and production, and the SHAKE algorithm[20] for hydrogen bonds was used for stabilization and production. Stabilization and equilibration were checked by monitoring density and temperature, which were found to remain close to equilibrium values. The use of the NPT samples was particularly important

for ensuring good convergence and averaging for calculations involving oxygen. Trajectories were analyzed using the MDAnalysis package.[22]

The procedure for calculating the CSA relaxation contribution was similar to the one used previously.[23] From the production run at 220 K, we extracted 100 random conformations of the molecule, and performed a geometry optimization using the B3LYP DFT functional, a 6-31G(d) basis set, and implicit chloroform solvent using Gaussian16 software[24] to find the local minimum. Convergence was checked *via* a frequency calculation. From these converged structures, we calculated CSA tensors using the same functional and basis set. The CSA tensors were separated into their traceless symmetric and antisymmetric components. For the relaxation expressions, two types of averages of the tensor norms were calculated: (1) individual tensor norm averages for spin–lattice relaxation rate constant (R_1) calculations, and (2) the averages of the norms of the differences of the tensors of the two proton nuclei for SO relaxation rate constant (R_S) calculations. The obtained tensor norms are shown in Fig. S4 (ESI†).

For correlation function calculations, 500 random starting points were chosen from trajectories and the results averaged. Each correlation function was calculated over 4000 points (800 ps).

To improve statistics, the correlation functions for spin-pairs were averaged for calculations obtained from switching the x, y, and z axes when calculating the P_2 function values.

Fig. 2 shows representative snapshots with a visualization of both the symmetric and the antisymmetric components of the CSA tensors. The symmetric CSA tensors were visualized with SpinDynamica v. 3.6[25] using the function Ovaloid (which was based on the procedure described previously[26,27]), and molecular graphics were created using Mathematicas Molecule visualization function. The antisymmetric tensor was visualized as follows:[28,29] the antisymmetric tensor σ_{anti} can be written as

$$\begin{pmatrix} 0 & -z & y \\ z & 0 & x \\ -y & -x & 0 \end{pmatrix}, \quad (1)$$

which can be recast in vector form $v = (x, y, z)$ and represented by the arrows shown in Fig. 2b. The antisymmetric shielding tensors are found to vanish if the H–C═C–H moiety is in a single plane.

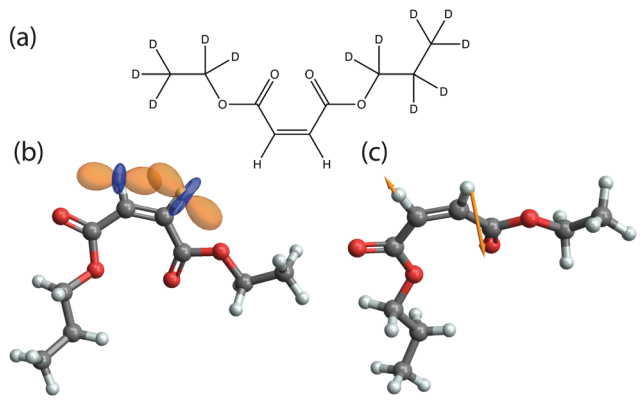

Fig. 2 (a) Ethyl-d_5 propyl-d_7 maleate (EPM) molecule. Singlet order was prepared for the vinylene protons in the center. (b) Representation of the symmetric CSA tensor components as ovaloid surfaces centred at the vinylene proton positions, and (c) representation of the antisymmetric CSA tensor components by arrows originating from the vinylene proton positions.

3 Results and discussion

We first discuss the analysis of R_1 relaxation mechanisms for $CHCl_3$ in the solvent because these are used as a benchmark, and also serve to determine the relative contribution of the paramagnetic mechanism due to oxygen, which is needed subsequently for the calculation the SO relaxation rate constant R_S.

3.1 Solvent relaxation

Fig. 3 shows the measured chloroform ^{1}H R_1 rate constants in the degassed solution, as well as the calculated rate constants for the main relaxation mechanisms. The relaxation mechanisms of chloroform have been studied previously,[30,31] and the main contributions have been determined as arising from the intra- and intermolecular dipolar coupling (to ^{2}H, ^{35}Cl, and ^{37}Cl), as well as the spin-rotation interaction. We believe, however, that the contribution of oxygen has previously not been determined. It is well-known that in a nondegassed sample, the paramagnetic mechanism accounts for the majority of the effect. In the degassed sample used in this study, the oxygen concentration is not known, but since one can calculate the dipolar coupling and the spin-rotation mechanisms from MD and *ab initio* simulations, one can assume that the remaining contribution must be due to oxygen.

3.1.1 Dipolar relaxation. Fig. 3a shows the contributions of the different dipolar mechanisms. It is observed here that the dipolar mechanisms due to ^{35}Cl and ^{37}Cl are much stronger that those due to ^{2}H. The reason is that there is no intramolecular mechanism due to ^{2}H, but more importantly, there are three times as many chlorine spins than there are ^{2}H spins, and their spin value is larger as well. Overall, this combination of factors explains the large contribution from chlorine spins as shown in Fig. 3a.

The dipolar contribution was calculated for ^{1}H–^{2}H, ^{1}H–^{35}Cl, and ^{1}H–^{37}Cl spin pairs using the following expression:[32]

$$R_1 = \frac{2}{3}\left(\frac{\mu_0}{4\pi}\hbar\gamma_I\gamma_S\right)^2 \times S(S+1)(J(|\omega_I - \omega_S|) + 3J(\omega_I) + 6J(\omega_I + \omega_S)), \quad (2)$$

where μ_0 is the permeability of vacuum, I and S are the spin values, $\gamma_{I,S}$ are the gyromagnetic ratios, the index I refers to the spin species for which the relaxation is being determined (here ^{1}H), and S to the spin whose dipolar coupling to spin I is the

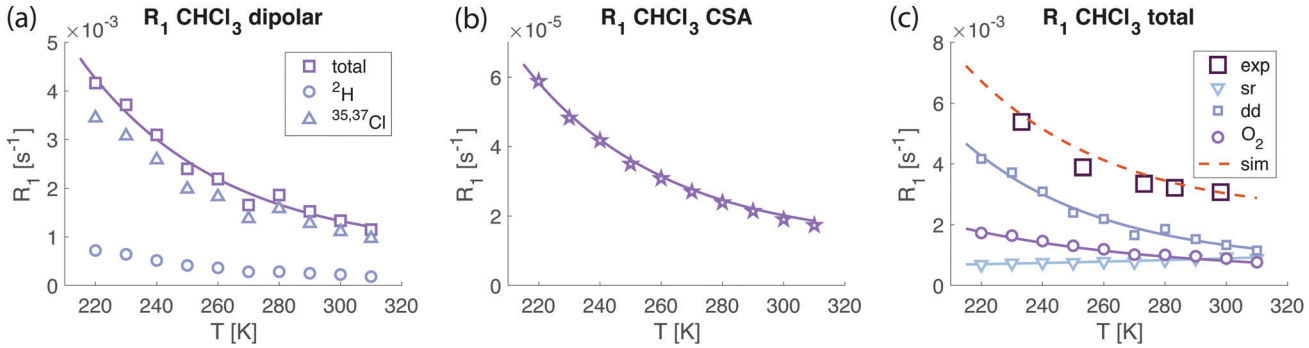

Fig. 3 Measured and calculated ^{1}H R_1 rate constants for $CHCl_3$ (in $CDCl_3$). (a) Components of the dipolar coupling mechanism showing the ^{1}H–^{2}H and the ^{1}H–^{35,37}Cl contributions. (b) CSA relaxation contribution (only the symmetric component is non-zero for chloroform). (c) Spin-rotation (sr), dipolar coupling (dd), paramagnetic (O_2) contributions, and their sum (red dashed line, labeled 'sim'), along with the experimentally determined values (exp).

cause of the mechanism. $\omega_{I,S}$ are the respective (angular) Larmor frequencies. The natural abundance values for the ^{35}Cl and ^{37}Cl spins (24.22 : 75.78) were used in averaging the chlorine contribution (both isotopes have the same spin = 3/2).

$J(\omega)$ is the spectral density function given *via* the Fourier transformation of the second-rank correlation function $C_2(t)$,

$$J(\omega) = \mathrm{Re}\left\{\int_0^\infty C_2(t)\exp(-i\omega t)\mathrm{d}t\right\}. \quad (3)$$

The function $C_2(t)$ is calculated from the MD trajectories using

$$C_2(t) = \overline{a_2(t')^* a_2(t+t')}, \quad (4)$$

where the average is performed over t', with

$$a_2(t) = P_2(\cos(\theta_{IS}))/{r_{IS}}^3. \quad (5)$$

θ_{IS} is the angle that the inter-spin vector makes with the z axis, P_2 is the second-order Legendre polynomial, and r_{IS} is the internuclear distance.

In this study, the largest correlation time was determined for the ^{1}H–^{35,37}Cl coupling for the lowest examined temperature (220 K). For this situation, we show the correlation function in Fig. S2 (ESI†). This curve can be fit very well with a biexponential function to give the two correlation times, 77.3 ps and 11.1 ps (with the longer correlation time accounting for approximately 40% of the amplitude). Using eqn (2), we can determine that using the fast motion regime would overestimate the rate by 2.4%. The overestimate is of course much smaller as the temperature increases, so this value could serve as an upper bound. Therefore, the fast motion regime can be applied to simplify the expressions for the system considered. This approach also avoids the use of any particular correlation function model (*e.g.* exponential decay), and one can hence make the approximation

$$J(\omega) \approx J(0) = \mathrm{Re}\left\{\int_0^\infty C(t)\mathrm{d}t\right\}. \quad (6)$$

The integration was performed to an upper limit of 800 ps in this study.

The same equations and procedures were used for both intra- and intermolecular processes, except for the following additional considerations for the latter: we analyzed the convergence behavior of the relaxation expressions when choosing particular cutoff distances for choosing intermolecular coupling partners. As seen in Fig. S3 (ESI†), a cutoff distance of 20 Å represents well-converged results, and hence this value was chosen for the cutoff distance. The difference in value between a 20 Å and 31 Å cutoff is below 1%.

3.1.2 CSA relaxation. Fig. 3b shows estimates of the CSA contributions to the R_1 rate constant for ^{1}H relaxation in $CHCl_3$. The CSA contribution is estimated to be approximately a factor 100 smaller than other contributions, as seen in Fig. 3b. Only the symmetric tensor is non-zero for the ^{1}H chloroform spin and $\|\sigma_{\mathrm{sym}}\|_F$ is found to be approximately 3.05 ppm. The relaxation rates for the CSA mechanism were calculated using the tensors determined from MD simulations by the expressions given in the ESI.†

3.1.3 Spin-rotation relaxation. In Fig. 3c we show the spin-rotation contribution, the overall dipolar contribution, as well as the paramagnetic relaxation contribution, compared to the experimentally determined values.

The expression for the spin-rotation relaxation can be obtained for a spherical top molecule (such as chloroform) using ref. 33 and 34 in terms of the principal components of the moments of inertia ($I_\perp$, $I_\parallel$) and diffusion tensors ($D_\perp$, $D_\parallel$) as

$$R_1^{\mathrm{sr}} = \frac{2}{3\hbar^2}\left({I_\parallel}^2{C_\parallel}^2 D_\parallel + 2{I_\perp}^2{C_\perp}^2 D_\perp\right). \quad (7)$$

A derivation of this expression is given in the ESI.†

Eqn (6.27) of Kowalewski and Mäler[34] may be adapted to give the following relationship between the diffusion constants and small orientational changes:

$$D_\parallel \simeq \frac{\delta\theta_\parallel^2}{\delta t} \quad (8)$$

$$D_\perp \simeq \frac{\delta{\theta_\perp}^2}{\delta t}. \quad (9)$$

Here $\delta\theta_\parallel$ and $\delta\theta_\perp$ are small rotation angles parallel and perpendicular to the symmetry axis, respectively, accumulated over a small time interval δt (which is 0.2 ps in this case).

The spin-rotation tensor components for chloroform are well-known, but can also be straightforwardly calculated. The values obtained using Gaussian16 were $C_{\parallel}/2\pi$ = 100 Hz, and $C_{\perp}/2\pi$ = 300 Hz, respectively. Note that some published expressions for spin-rotation relaxation contain errors in the numerical factors.[30,31]

3.1.4 Paramagnetic relaxation due to O_2. The relaxation of nuclei by the interaction with unpaired electrons is a complex topic.[35,36] A detailed treatment of this problem requires good understanding of the electron spin interactions including zero-field splittings. For the sake of tractability, we employed a simplified treatment based on Solomon relaxation of the O_2 electron spin pair. The relaxation contribution was determined by first calculating $R_1^{O_2,dd}$, the dipolar coupling contribution by the procedure outlined above, with S = 1 for the unpaired electrons of O_2, and using the gyromagnetic ratio for the electron. The correlation time for this mechanism, $\tau^{O_2,dd}$, was then adjusted to obtain an effective correlation time $\tau^{O_2,eff}$ in order to incorporate the effect of the electron spin–lattice relaxation time T_{1e}, according to

$$\frac{1}{\tau^{O_2,eff}} = \frac{1}{\tau^{O_2,dd}} + \frac{1}{T_{1e}}. \quad (10)$$

The electron relaxation time T_{1e} was recently reported to be 7.5 ps for most organic solvents at room temperature,[37] which is the value we used. We note that an increase of T_{1e} would lead to larger rate constants, and hence to a decrease in the determined oxygen concentration. The ESI† contains an evaluation of the influence of T_{1e} on the paramagnetic relaxation contribution (Fig. S5, ESI†). The scaling factor determined from R_1 data was subsequently used to scale the computed interaction for the contribution to the SO relaxation rate constant R_S. As a result, we obtain a self-consistent procedure for determining the paramagnetic relaxation contribution to R_S. Further details on the calculation of the paramagnetic mechanism, and the influence of T_{1e} on the rate constants are shown in ESI.†

3.1.5 Consideration of further contributions. One may also consider the potential effect of ^{1}H–^{1}H dipolar coupling due to the fraction of protonated solvent (<0.2%). We can estimate the size of this contribution from the ^{1}H–^{2}H dipolar coupling contribution as follows: The largest R_1 rate constant due to ^{2}H is 7.2 × 10^{-4} s^{-1}. The factor

$$c_{HD} = (\gamma_D/\gamma_H)^2 \frac{I_D(I_D+1)}{I_H(I_H+1)} = 0.0628 \quad (11)$$

represents the conversion factor between the relaxation rate constants due to proton and deuterium (I_D = 1 and I_H = 1/2 are the spin values of ^{2}H and ^{1}H, respectively). Therefore, the estimate of the effect of residual ^{1}H on chloroform R_1 is 7.2 × 10^{-4}·0.002/c_{HD} = 2.29 × 10^{-5} s^{-1}. This rate constant is clearly negligible (more than a factor 100 smaller than the smallest calculated contribution to R_1).

3.2 Singlet order relaxation

Next, we turn our attention to the measurement and computation of SO relaxation rate constants R_S for the vinylene protons in the EPM molecule. To measure the singlet lifetimes we used an M2S pulse sequence with 25 pulse composite 180 pulses, which were previously shown to alleviate any potential complications from convection in the sample, in particular in the measurement of very long singlet lifetimes.[18] A zero-rank tensor filter[19] (subsequently referred to as T00 filter) as shown in Fig. 1 was used to remove spin order other than SO up to rank two. Convection was further controlled by restricting the height of the solution in the NMR tube to within the active rf coil volume.[18]

The ESI† includes a comparison between experimental and computed vinylene R_1 rates, which demonstrate the legitimacy of the computed rotational correlation times, which indicates that the dynamics of this molecule appear to be captured well by MD simulations (Fig. S6, ESI†).

Fig. 4 compares the experimentally measured R_S rate constants for the vinylene protons of EPM with the computed ones, and shows the contributions of the different mechanisms.

3.2.1 Dipolar relaxation. Fig. 4a shows the individual contributions of the different dipolar coupling mechanisms, including both intra- and intermolecular ones. As for the R_1 calculation above, it is observed here that the interactions with ^{35}Cl, and ^{37}Cl are much stronger overall than those with ^{2}H, although the difference is not as large as seen for chloroform

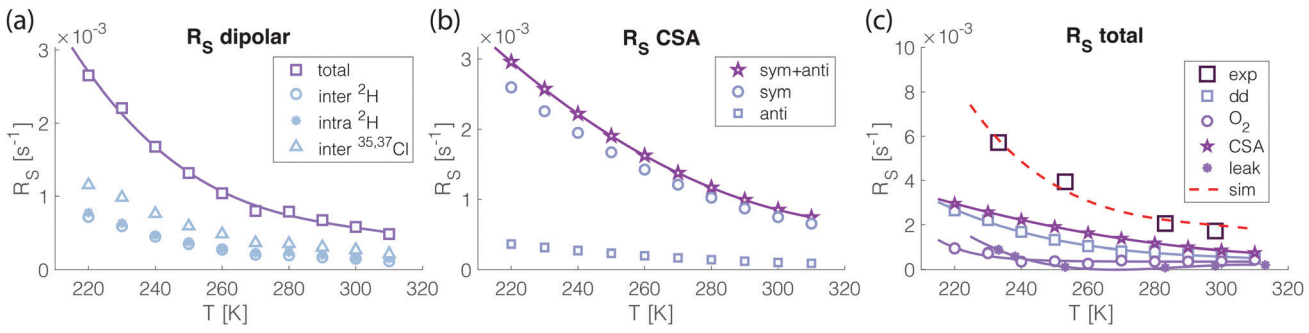

Fig. 4 Measured and calculated R_S rate constants for the vinylene protons in EPM in $CDCl_3$. (a) Components of the dipolar coupling mechanism showing the intra- and intermolecular ^{1}H–^{2}H, and the intermolecular ^{1}H–^{35,37}Cl contributions. (b) Symmetric (sym) and antisymmetric (anti) CSA relaxation contributions. (c) CSA, dipolar coupling (dd), paramagnetic (O_2), singlet–triplet leakage (leak) contributions, and their sum (red dashed line, labeled 'sim'), along with the experimentally determined values (exp).

R_1. Both the intra- and intermolecular ^{2}H interactions are of a similar level, approximately at 70% of the interactions with chlorine spins.

R_S rate constants due to dipolar coupling were calculated as follows: although it is not difficult, in principle, to calculate the exact relaxation rate constant according to the equations given by Pileio,[38] a more efficient algorithm can be used when the fast motion approximation applies. The justification for the use of the fast motion regime was already discussed above and is corroborated by the data provided in Fig. S2 (ESI†).

SO relaxation rate constants due to dipolar coupling were calculated in this regime by

$$R_S = \frac{20}{3}\left(\frac{\mu_0}{4\pi}\hbar\gamma_I\gamma_S\right)^2 S(S+1)J(0), \quad (12)$$

where the spectral density function relates to the correlation function *via* eqn (6). The correlation function is calculated in this case by

$$C_2(t) = C_{SO}(t) = \overline{a^*_{SO}(t'+t)a_{SO}(t')}, \quad (13)$$

where

$$a_{SO}(t) = P_2(\cos(\theta_{I1S}))/r_{I1S}{}^3 - P_2(\cos(\theta_{I2S}))/r_{I2S}{}^3, \quad (14)$$

with the subscripts to I and r indicating for which spin of the two vinylene spins the quantities are evaluated. The paramagnetic contribution to R_S was calculated using the same expressions as for dipolar coupling, with the substitutions for the spin value ($S = 1$) and the electron gyromagnetic ratio. In addition, a correction for T_{1e} was performed in analogy to eqn (10).

3.2.2 CSA relaxation. Fig. 4b shows the calculated CSA contribution to R_S performed from MD snapshots according to the procedure given in the ESI† document. The CSA difference tensor norms were found to be $\|\Delta\sigma_{sym}\|_F$ = 4.35 ppm and $\|\Delta\sigma_{anti}\|_F$ = 0.94 ppm. The standard deviations of 0.13 and 0.18 ppm, respectively, indicate that the values do not fluctuate significantly, especially for the symmetric component. The tensor norms of these difference tensors are shown in Fig. S4 (ESI†). It is seen that the contribution from the symmetric interaction is significantly stronger than the antisymmetric one.

3.2.3 Paramagnetic relaxation due to O_2. Fig. 4c shows all the mechanisms (including the paramagnetic interaction due to oxygen) together, as well as their sum. It is seen that the calculated rate constants track the experimentally observed very well. This result is of particular interest, given that no adjustable parameters were used. Fig. 4c also shows that overall, the effect of oxygen is relatively minor, but not negligible. The level of the relaxation mechanism, however, is a testament to the importance of thorough oxygen removal for the measurement of long singlet lifetimes, as an oxygen concentration that would be higher by a factor three would eclipse the dipolar contribution.

3.2.4 Singlet–triplet leakage. Since there is a non-negligible chemical shift difference between the vinylene proton spins, there is the possibility that singlet order may leak into triplet states.[39] The chemical shift differences $\Delta\delta$ are relatively small compared to the intra-vinyl J-coupling. Both $\Delta\delta$ and J can be determined from the optimized M2S pulse sequence parameters, in particular from the delays Δ, and the cycle numbers n_1 as described by Pileio *et al.*[40] The intra-vinylene J-coupling was determined as ranging from 12.1–12.3 Hz, and the chemical shift differences $\Delta\delta$ determined in this way are shown in Fig. S1 (ESI†), with the maximum reaching approximately 1.9 Hz at the lowest temperature. The contribution from singlet–triplet leakage was determined by calculating the SO decay using Spinach,[41] with a vinylene J-coupling constant of 12.1 Hz, the chemical shift differences of Fig. S1 (ESI†), and the rotational correlation times determined from the results shown in Fig. S6 (ESI†). The resulting singlet–triplet rates are shown in Fig. 4c. A significant contribution from this effect is only observed at the lowest temperature (due to the long correlation time at this temperature). This contribution is still significantly smaller than either the CSA or the dipolar coupling contributions.

3.2.5 Consideration of further contributions. As above, one can estimate the potential contribution of residual ^{1}H in deuterated chloroform: The largest R_S rate constant due to intermolecular dipolar coupling with ^{2}H is 7.77×10^{-4} s^{-1}. Considering a fraction of 0.2% ^{1}H in the solvent, the estimate of the effect of residual solvent ^{1}H on EPM R_S is $7.77 \times 10^{-4} \cdot 0.002$ s$^{-1}/c_{HD} = 2.47 \times 10^{-5}$ s^{-1}, which is more than a factor 100 smaller than the smallest dipolar coupling contribution to R_S calculated above.

Furthermore, we consider whether EPM-EPM dipolar interactions could play a role. An estimate of such potential contributions could be obtained as follows: The EPM concentration is 5.4 mM. There are two ^{1}H spins in the deuterated EPM molecule that we use. The concentration of neat $CDCl_3$ is ~13 M. We calculated above the relaxation contributions due to a 0.2% of that amount (corresponding to the residual ^{1}H content). Therefore, any dipolar contribution from distant EPM molecules would be scaled by a factor of $2 \cdot 0.0054/(13 \cdot 0.002) = 0.415$ from the rate constant considered in the previous paragraph. Hence this contribution can be approximated to be at a level of 1×10^{-5} s^{-1} for EPM R_S, which we can also safely neglect.

The spin-rotation contribution, while important for $CHCl_3$ relaxation, does not play a role for larger solvated molecules such as EPM. This mechanism could, however, be an important one to consider for hyperpolarized gas-phase molecules such as propane and diethyl ether.[42,43]

The contributions to R_S from dipolar coupling and the CSA interaction are the largest and are roughly of the same order over the whole temperature range. It is of note that one could remove the CSA interaction by reducing the external field. It is interesting to estimate the limit of singlet lifetimes under such conditions. For the molecule examined here, the strongest contribution would then be given by dipolar coupling, which would produce lifetime limits of 578 s at 220 K and 1127 s at 300 K. It is of note that the biggest component thereof is given by the intermolecular coupling to chlorine spins, something that is rarely being considered. Since singlet NMR typically

requires a solvent, one can see such interactions as presenting hard limits to singlet lifetimes. From the effect on ^{1}H, one can further deduce expected limits for singlet lifetimes for other nuclear species. For example, the record for organic molecules has been established as over an hour for ^{13}C spin pairs.[3,44] From our results for ^{1}H spins, we could estimate the approximate SO lifetime limits due to solvent interactions for ^{13}C spins: we obtain a SO lifetime limit for ^{13}C spins due to $CDCl_3$ solvent of approximately 1.2 h, if we only consider the relative γ factor. The lifetime limit would likely be a little longer because the distance of closest approach would be larger for ^{13}C spins. Nonetheless, this consideration appears to indicate that the lifetimes observed thus far in the literature may already be very close to the theoretical limits given by solvent effects. This finding may also be an additional motivation to opt for supercritical CO_2 as a solvent.[44]

4 Conclusions

In summary, we discuss here results from an experimental and computational study of different nuclear spin singlet relaxation mechanisms in order to reproduce the temperature behavior of experimentally observed relaxation rate constants of an organic molecule in solution. In particular, it is shown that a combination of intra- and intermolecular dipolar coupling relaxation (^{1}H–^{2}H, ^{1}H–^{35,37}Cl), chemical shift anisotropy (both symmetric and antisymmetric), as well as a relatively minor contribution from paramagnetic relaxation due to residual oxygen can fully account for the observed rate constants of an organic molecule in solution. Self-consistency in the predictions is achieved by examining the solvent relaxation in order to determine the contribution of oxygen to relaxation. This study further identifies potentially hard limits on nuclear spin singlet relaxation rate constants given by solvent interactions (even in deuterated solvents), which may set an upper boundary on singlet lifetimes in solution.

Conflicts of interest

There are no conflicts to declare.

Acknowledgements

AJ acknowledges funding through an award of the U.S. National Science Foundation, award no. CHE 2108205, an award by the Heising-Simons Foundation. AJ acknowledges the receipt of a Diamond Jubilee Visiting Fellowship to the University of Southampton. This work was supported in part through the NYU IT High Performance Computing resources, services, and staff expertise (in particular by Dr Shenglong Wang). During manuscript preparation, B.B. Kharkov was supported by grant 72777155 from St. Petersburg State University awarded to the Laboratory of Biomolecular NMR at SPbSU. This research was further supported by EPSRC-UK (grant numbers EP/P009980/1, EP/T004320/1 and EP/P030491/1), and the European Unions Horizon 2020 research and innovation programme under the Marie Skłodowska-Curie grant agreement No 891400, and the European Research Council (grant 786707-FunMagResBeacons). We thank Harry Harbor Collins for pointing us to a typo in eqn (10), which we were able to correct at proof stage. We acknowledge extensive discussions with Dr Christian Bengs with regard to nuclear spin singlet relaxation mechanisms.

Notes and references

1 M. Carravetta, O. G. Johannessen and M. H. Levitt, *Phys. Rev. Lett.*, 2004, **92**, 153003.
2 M. Carravetta and M. H. Levitt, *J. Am. Chem. Soc.*, 2004, **126**, 6228–6229.
3 G. Stevanato, J. T. Hill-Cousins, P. Hakansson, S. S. Roy, L. J. Brown, R. C. Brown, G. Pileio and M. H. Levitt, *Angew. Chem., Int. Ed.*, 2015, **54**, 3740–3743.
4 G. Pileio, S. Bowen, C. Laustsen, M. C. Tayler, J. T. Hill-Cousins, L. J. Brown, R. C. Brown, J. H. Ardenkjaer-Larsen and M. H. Levitt, *J. Am. Chem. Soc.*, 2013, **135**, 5084–5088.
5 S. Cavadini, J. Dittmer, S. Antonijevic and G. Bodenhausen, *J. Am. Chem. Soc.*, 2005, **127**, 15744–15748.
6 R. Sarkar, P. R. Vasos and G. Bodenhausen, *J. Am. Chem. Soc.*, 2007, **129**, 328–334.
7 Y. Zhang, X. Duan, P. C. Soon, V. Sychrovsky, J. W. Canary and A. Jerschow, *ChemPhysChem*, 2016, **17**, 2967–2971.
8 S. J. Elliott, L. J. Brown, J.-N. Dumez and M. H. Levitt, *J. Magn. Reson.*, 2016, **272**, 87–90.
9 A. Philips and J. Autschbach, *Phys. Chem. Chem. Phys.*, 2019, **21**, 26621–26629.
10 S. Badu, L. Truflandier and J. Autschbach, *J. Chem. Theory Comput.*, 2013, **9**, 4074–4086.
11 A. Carof, M. Salanne, T. Charpentier and B. Rotenberg, *J. Chem. Phys.*, 2016, **145**, 124508–124509.
12 M. Mohammadi, S. Benders and A. Jerschow, *J. Chem. Phys.*, 2020, **153**, 184502.
13 R. Brüschweiler, *Curr. Opin. Struct. Biol.*, 2003, **13**, 175–183.
14 M. Odelius, A. Laaksonen, M. H. Levitt and J. Kowalewski, *J. Magn. Reson., Ser. A*, 1993, **105**, 289–294.
15 M. Odelius, C. Ribbing and J. Kowalewski, *J. Chem. Phys.*, 1996, **104**, 3181–3188.
16 P. Håkansson, *Phys. Chem. Chem. Phys.*, 2017, 1–18.
17 G. Stevanato, S. S. Roy, J. Hill-Cousins, I. Kuprov, L. J. Brown, R. C. Brown, G. Pileio and M. H. Levitt, *Phys. Chem. Chem. Phys.*, 2015, **17**, 5913–5922.
18 B. Kharkov, X. Duan, J. W. Canary and A. Jerschow, *J. Magn. Reson.*, 2017, **284**, 1–7.
19 G. Pileio and M. H. Levitt, *J. Magn. Reson.*, 2008, **191**, 148–155.
20 D. A. Case, I. Y. Ben-Shalom, S. R. Brozell, D. S. Cerutti, T. E. Cheatham III, V. W. D. Cruzeiro, T. A. Darden, R. E. Duke, D. Ghoreishi, G. Giambasu, T. Giese, M. K. Gilson, H. Gohlke, A. W. Goetz, D. Greene, R. Harris, N. Homeyer, Y. Huang, S. Izadi, A. Kovalenko, R. Krasny, T. Kurtzman, T. S. Lee, S. LeGrand, P. Li, C. Lin, J. Liu, T. Luchko, R. Luo, V. Man, D. J. Mermelstein, K. M. Merz, Y. Miao, G. Monard,

C. Nguyen, H. Nguyen, A. Onufriev, F. Pan, R. Qi, D. R. Roe, A. Roitberg, C. Sagui, S. Schott-Verdugo, J. Shen, C. Simmerling, J. Smith, J. Swails, R. C. Walker, J. Wang, H. Wei, L. Wilson, R. M. Wolf, X. Wu, L. Xiao, Y. Xiong, D. M. York and P. A. Kollman, *AMBER 2020*.

21 J. Wang, R. M. Wolf, J. W. Caldwell, P. A. Kollman and D. A. Case, *J. Comput. Chem.*, 2004, **25**, 1157–1174.

22 N. Michaud-Agrawal, E. J. Denning, T. B. Woolf and O. Beckstein, *J. Comput. Chem.*, 2011, **32**, 2319–2327.

23 D. E. Korenchan, J. Lu, M. H. Levitt and A. Jerschow, *Phys. Chem. Chem. Phys.*, 2021, **23**, 19465–19471.

24 M. J. Frisch, G. W. Trucks, H. B. Schlegel, G. E. Scuseria, M. A. Robb, J. R. Cheeseman, G. Scalmani, V. Barone, G. A. Petersson, H. Nakatsuji, X. Li, M. Caricato, A. V. Marenich, J. Bloino, B. G. Janesko, R. Gomperts, B. Mennucci, H. P. Hratchian, J. V. Ortiz, A. F. Izmaylov, J. L. Sonnenberg, D. Williams-Young, F. Ding, F. Lipparini, F. Egidi, J. Goings, B. Peng, A. Petrone, T. Henderson, D. Ranasinghe, V. G. Zakrzewski, J. Gao, N. Rega, G. Zheng, W. Liang, M. Hada, M. Ehara, K. Toyota, R. Fukuda, J. Hasegawa, M. Ishida, T. Nakajima, Y. Honda, O. Kitao, H. Nakai, T. Vreven, K. Throssell, J. A. Montgomery, Jr., J. E. Peralta, F. Ogliaro, M. J. Bearpark, J. J. Heyd, E. N. Brothers, K. N. Kudin, V. N. Staroverov, T. A. Keith, R. Kobayashi, J. Normand, K. Raghavachari, A. P. Rendell, J. C. Burant, S. S. Iyengar, J. Tomasi, M. Cossi, J. M. Millam, M. Klene, C. Adamo, R. Cammi, J. W. Ochterski, R. L. Martin, K. Morokuma, O. Farkas, J. B. Foresman and D. J. Fox, *Gaussian 16 Revision C.01*, Gaussian Inc., Wallingford CT, 2016.

25 C. Bengs and M. H. Levitt, *Magn. Reson. Chem.*, 2018, **56**, 374–414.

26 R. Radeglia, *Solid State Nucl. Magn. Reson.*, 1995, **4**, 317–321.

27 R. P. Young, C. R. Lewis, C. Yang, L. Wang, J. K. Harper and L. J. Mueller, *Magn. Reson. Chem.*, 2019, **57**, 211–223.

28 A. Buckingham and S. Malm, *Mol. Phys.*, 1971, **22**, 1127–1130.

29 F. A. L. Anet and D. J. O'Leary, *Concepts Magn. Reson.*, 1991, **3**, 193–214.

30 Dinesh and M. T. Rogers, *J. Chem. Phys.*, 1972, **56**, 542.

31 H. J. Bender and M. D. Zeidler, *Ber. Bunsenges. Phys. Chem.*, 1971, **75**, 236–242.

32 J. Cavanagh, W. J. Fairbrother, A. G. Palmer III and N. J. Skelton, *Protein NMR spectroscopy: principles and practice*, Elsevier, 1995.

33 R. E. D. McClung, *Spin–Rotation Relaxation Theory*, John Wiley & Sons, Ltd, Chichester, UK, 2007, vol. 91.

34 J. Kowalewski and L. Mäler, *Nuclear spin relaxation in liquids: theory, experiments, and applications*, CRC Press, 2nd edn, 2017.

35 J. Kowalewski, D. Kruk and G. Parigi, *Adv Inorg. Chem.*, Elsevier, 2005, vol. 57, pp. 41–104.

36 J. Kowalewski, L. Nordenskiöld, N. Benetis and P.-O. Westlund, *Prog. Nucl. Magn. Reson. Spectrosc.*, 1985, **17**, 141–185.

37 C. L. Teng, H. Hong, S. Kiihne and R. G. Bryant, *J. Magn. Reson.*, 2001, **148**, 31–34.

38 G. Pileio, *J. Chem. Phys.*, 2011, **134**, 214505–214510.

39 B. Kharkov, X. Duan, E. S. Tovar, J. W. Canary and A. Jerschow, *Phys. Chem. Chem. Phys.*, 2019, **21**, 2595–2600.

40 G. Pileio, M. Carravetta and M. H. Levitt, *Proc. Natl. Acad. Sci. U. S. A.*, 2010, **107**, 17135–17139.

41 H. J. Hogben, M. Krzystyniak, G. T. Charnock, P. J. Hore and I. Kuprov, *J. Magn. Reson.*, 2011, **208**, 179–194.

42 O. G. Salnikov, A. Svyatova, L. M. Kovtunova, N. V. Chukanov, V. I. Bukhtiyarov, K. V. Kovtunov, E. Y. Chekmenev and I. V. Koptyug, *Chem. – Eur. J.*, 2021, **27**, 1316–1322.

43 D. B. Burueva, V. P. Kozinenko, S. V. Sviyazov, L. M. Kovtunova, V. I. Bukhtiyarov, E. Y. Chekmenev, O. G. Salnikov, K. V. Kovtunov and I. V. Koptyug, *Appl. Magn. Reson.*, 2021, 1–17.

44 A. Moysiadi, F. Giustiniano, A. M. R. Hall, T. A. A. Cartlidge, L. J. Brown and G. Pileio, *Front. Chem.*, 2021, **9**, 243.

